Structure of liquid water at high pressures and temperatures

2002 J. Phys.: Condens. Matter 14 11385

(http://iopscience.iop.org/0953-8984/14/44/487)

INSTITUTE OF PHYSICS PUBLISHING JOURNAL OF PHYSICS: CONDENSED MATTER

J. Phys.: Condens. Matter **14** (2002) 11385–11394 PII: S0953-8984(02)38320-6

Structure of liquid water at high pressures and temperatures

Jon H Eggert[1,2], **Gunnar Weck**[2] **and Paul Loubeyre**[2]

[1] Lawrence Livermore National Laboratory, PO Box 808, Livermore, CA 94550, USA
[2] DIF/DPTA/SPMC, CEA, 91680 Bruyères-le-Châtel, France

Received 18 June 2002
Published 25 October 2002
Online at stacks.iop.org/JPhysCM/14/11385

Abstract
We report quantitatively accurate structure-factor and radial-distribution-function measurements of liquid water in a diamond-anvil cell (DAC) using x-ray diffraction. During the analysis of our diffraction data, we found it possible (and necessary) to also determine the density. Thus, we believe we present the first-ever diffraction-based determination of a liquid structure factor and equation of state in a DAC experiment.

1. Introduction

The experimental study of the structure of liquids at high pressures and temperatures has been a long-standing goal of high-pressure research. With the maturation of third-generation synchrotron sources this goal is now attainable. We report measurements of the structure factor, radial-distribution function, and density of liquid water at room temperature up to 1.1 GPa by angle-dispersive x-ray diffraction.

A major difficulty with liquid diffraction at high pressure is the large background signal generated by the pressure vessel. In large-volume cells this can be overcome using energy-dispersive diffraction and careful spatial filtering of the scattered radiation [1], or using angle-dispersive diffraction and precise Soller slits [2]. Unfortunately, low-Z compressible liquids and gases are much easier to study in diamond-anvil cells (DACs) and neither approach is possible with the much smaller sample volumes required for DAC studies. Quantitative structural information on liquids has never before been obtained in DAC experiments. In addition to our results on water, we report briefly on the analytical procedure that has enabled us to extract such information from both atomic and molecular liquids. A more detailed derivation will be published separately [3].

2. Experimental details

Using standard procedures, we loaded high-purity water into specially-modified membrane-diamond-anvil cells (MDACs) [4] with large-angle access $2\theta_{max} = 36°$ as shown in figure 1.

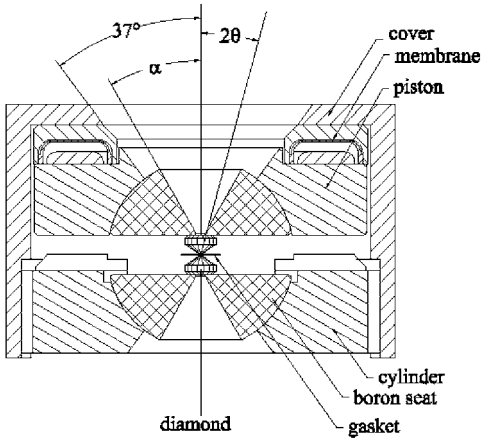

Figure 1. Diagram of the MDAC.

The diamond-anvil seats were made of boron to give high x-ray transmission over the full aperture of the MDAC.

We performed angle-dispersive x-ray diffraction on the ID09 and ID30 beam lines at the European Synchrotron Radiation Facility (ESRF) using a doubly focused monochromatic beam with wavelength $\lambda = 0.3738$ Å. The beam was focused to a diameter of between 20 and 80 μm, depending on the sample size, to avoid contamination of the spectra by diffraction from the gasket. We used a MAR345 on-line scanning image-plate detector [5]. The sample–detector distance and the detector tilt angles were measured using diffraction from a silicon-powder standard. The x-ray beam was 99% horizontally polarized and all geometric and polarization corrections were made during angular integration.

Typical exposure times of 5 min were needed to achieve high exposure of the image plates while avoiding saturation. To obtain empty-cell backgrounds we generally had to disassemble the MDAC and reposition the cell as accurately as possible. To eliminate any Bragg diffraction from the diamonds we masked the Bragg peaks before performing the angular integrations, being sure to use the same mask for all the spectra in an experiment.

3. Analysis

Since the diffuse scattering in a DAC experiment is dominated by background scattering (by one or two orders of magnitude), our analysis is necessarily different than for most liquid-diffraction experiments where background scattering is minimized. Thus, we will briefly derive several general equations applicable to monatomic, and molecular, liquids so that our results can be clearly interpreted.

For a monatomic liquid the structure factor is defined as

$$S(Q) \equiv \frac{I^{coh}(Q)}{Nf^2(Q)} = 1 + \rho_0 \int_0^\infty [g(r) - 1] \frac{\sin Qr}{Qr} 4\pi r^2 \, \mathrm{d}r, \tag{1}$$

where $f(Q)$ is the atomic form factor, ρ_0 is the atomic density, and $g(r)$ is the radial-distribution function. Equation (1) can be Fourier transformed to find $g(r)$

$$F(r) = 4\pi r \rho_0 [g(r) - 1] = \frac{2}{\pi} \int_0^{Q_{max}} Q i(Q) \sin(Qr) \, \mathrm{d}Q, \tag{2}$$

where $i(Q) = S(Q) - 1$.

For molecular liquids, (1) cannot be straightforwardly transformed due to the difficulty of determining an accurate molecular form factor. In our treatment we define several common [6] effective molecular parameters: the effective electronic form factor

$$f_e(Q) = \frac{\sum f_p(Q)}{Z_{tot}},$$

where Z_{tot} is the total molecular atomic number; the effective atomic number

$$K_p = \left\langle \frac{f_p(Q)}{f_e(Q)} \right\rangle_Q,$$

where the angle brackets denote an average over the measured range of Q; and an effective molecular density function,

$$\rho_{mol}(r) = \sum\sum \frac{K_p K_q}{Z_{tot}^2} \rho_{p,q}(r), \tag{3}$$

where $\rho_{p,q}(r)$ is the density of atom centres of type q at a distance r from an atom of type p, with p and q denoting all the atoms in the molecule. We use the analytic tabulation of Hajdu [7] to evaluate the atomic form factors, $f_p(Q)$. With these definitions (1) becomes

$$S_{mol}(Q) \equiv \frac{I^{coh}(Q)}{N Z_{tot}^2 f_e^2(Q)} = S_\infty + \rho_0 \int_0^\infty [g_{mol}(r) - 1] \frac{\sin Qr}{Qr} 4\pi r^2 \, \mathrm{d}r, \tag{4}$$

where

$$S_\infty \equiv \frac{\sum K_p^2}{Z_{tot}^2}. \tag{5}$$

N is now the number of molecules, and ρ_0 is the molecular density. We can Fourier transform (4) to find

$$F(r) = 4\pi r \rho_0 [g_{mol}(r) - 1] = \frac{2}{\pi} \int_0^{Q_{max}} Q i(Q) \sin(Qr) \, \mathrm{d}Q, \tag{6}$$

where $i(Q) = S_{mol}(Q) - S_\infty$. Using (3) we identify our effective molecular radial distribution function as a linear combination of partial radial distribution functions

$$g_{mol}(r) = \sum\sum \frac{K_p K_q}{Z_{tot}^2} g_{p,q}(r), \tag{7}$$

to facilitate comparison with other experiments and simulations.

4. Data treatment

The experimental determination of $I^{coh}(Q)$ appearing in (4) is given by

$$I^{coh}(Q) = N\Big[\alpha I^{samp}(Q) - \sum I_p^{incoh}(Q)\Big], \tag{8}$$

where $I_p^{incoh}(Q)$ is the incoherent (Compton) scattering from atoms of type p in the sample computed using the analytic atomic formulae of Hajdu [7], α is a normalization factor to put the signal into atomic units, and

$$I^{samp}(Q) = \frac{I^{meas}(Q) - s I^{bkgd}(Q)}{T(Q)}. \tag{9}$$

$I^{meas}(Q)$ and $I^{bkgd}(Q)$ are obtained by ϕ-integration of the image-plate signal including a polarization correction, and $T(Q)$ is the MDAC transmission factor. $T(Q)$ was always greater than 90% in these experiments and was calculated based on the known MDAC geometry and

absorption of diamond and boron (including impurities). Reasonable errors in the magnitude and shape of $T(Q)$ had no affect on our results.

The proper determination of the reference background spectra $I^{bkgd}(Q)$ is the most difficult aspect of making and analysing these measurements. We attempted to minimize the background signal by using thick samples (up to 100 μm) and thin diamond anvils (down to 500 μm), but diffuse scattering from the diamonds was still dominant by more than an order of magnitude. Great care must be exercised in collecting the reference spectra with the gasket-hole shape, size, and position identical to that used for the liquid spectra. This is because the metallic gasket serves as an aperture for the diffuse scattering from the first diamond and the shape of $I^{bkgd}(Q)$ is intimately related to this aperture effect. Scattering from the diamond anvils takes the form of the following:

(i) Bragg scattering, which is easily removed by digitally masking the image integration;
(ii) Compton scattering, which is assumed to be independent of pressure and temperature; and
(iii) temperature-diffuse scattering (TDS), which is far more insidious due to its temperature dependence and anisotropy, necessitating a separate reference spectra for each sample temperature.

To simplify the collection of appropriate background spectra, we developed a procedure for utilizing solid-sample reference spectra. The most difficult aspect of using solid-sample references involves properly treating the sample TDS [3].

5. Optimization procedure

We determine the normalization factor α in (8) using the Krogh-Moe [8] and Norman [9] method

$$\alpha = \frac{-2\pi^2\rho_0 + \int_0^{Q_{max}} [J(Q) + S_\infty] Q^2 \, \mathrm{d}Q}{\int_0^{Q_{max}} L(Q) Q^2 \, \mathrm{d}Q}, \tag{10}$$

where

$$J(Q) \equiv \frac{\sum I_p^{incoh}(Q)}{Z_{tot}^2 f_e^2(Q)}, \qquad \text{and} \qquad L(Q) \equiv \frac{I^{samp}(Q)}{Z_{tot}^2 f_e^2(Q)}.$$

This equation is exact for infinite Q_{max}, but the limited experimental range of Q and the lack of knowledge of ρ_0 makes the determination of α uncertain. Due to the domination of the diffuse diamond background over scattering from the sample, we need to determine the scale factor s in (9) with high precision as well. Accurate direct measurement of the beam intensity is not currently possible on the beam lines we used, so an alternative method for finding s was needed.

We now present a self-consistent, corrective procedure that addresses the problems associated with uncertainties in α, s, and the form factor $f_e(r)$ (which does not take into account electronic bonding and charge-transfer effects) and even allows us to experimentally determine ρ_0. Following the general outline of a method for minimizing errors in the determination of $g(r)$ pioneered by Kaplow *et al* [10], we force the behaviour of $F(r)$ at small $r < r_{min}$ (below the first *inter*molecular peak) to match the expected behaviour for a given sample including peaks due to *intra*molecular interference in the frozen-atom approximation [3]. This involves an iterative procedure where the difference between the expected small-r behaviour and the

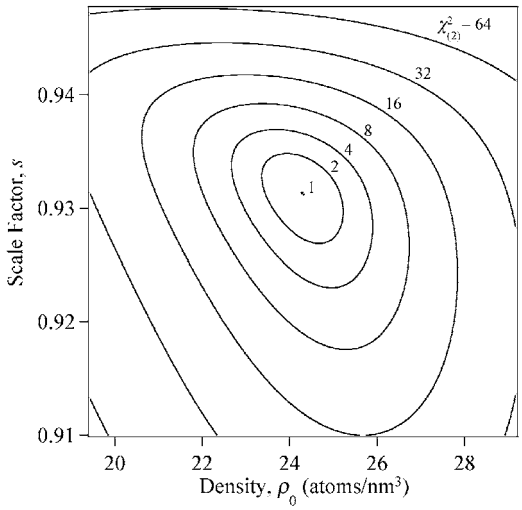

Figure 2. Contour plot of $\chi^2_{(2)}$. Note that $\chi^2_{(2)}$ has been normalized to 1 at the minimum.

actual $F(r)$ is inverse Fourier transformed to find an improved value of the structure factor according to the following equations:

$$\begin{aligned}
&(i) \quad F_{(i)}(r) = \frac{2}{\pi}\int_0^{Q_{max}} Q i_{(i)}(Q)\sin(Qr)\,\mathrm{d}Q,\\
&(ii) \quad \Delta F_{(i)}(r) = F_{(i)}(r) - [F_{intra}(r) - 4\pi r\rho_0],\\
&(iii) \quad i_{(i+1)}(Q) = i_{(i)}(Q) - \frac{1}{Q}\left[\frac{i_{(i)}(Q)}{S_\infty + J_0(Q)} + 1\right]\int_0^{r_{min}} \Delta F_{(i)}(r)\sin(Qr)\,\mathrm{d}r,
\end{aligned} \tag{11}$$

where $F_{intra}(r)$ is the frozen-atom contribution to $F(r)$. This procedure converges very rapidly and generally two iterations were sufficient for convergence [3].

As Kaplow originally noted [10], ρ_0 is an independent variable in this analysis with a direct influence on α and on $\Delta F_{(i)}(r)$, so that ρ_0 can be found by minimizing $\chi^2_{(i)} \equiv \int_0^{r_{min}} \Delta F^2_{(i)}(r)$. The optimum value for s can be found similarly. From this discussion it is not at all apparent that $\chi^2_{(i)}$ is sufficiently well behaved to allow the determination of either ρ_0 or s, not to mention both of them. However, it turns out that there is a unique, well defined minimum in $\chi^2_{(i)}$ and that the variables ρ_0 and s are surprisingly independent. This can be seen in figure 2 which shows a contour plot of $\chi^2_{(2)}$ in ρ_0, s space. The independence of ρ_0 and s is demonstrated by the nearly circular symmetry near the minimum of $\chi^2_{(2)}$. In fact, we are able to determine the minimum with a high degree of precision.

6. Results

Figure 3 shows the optimum density ρ_0 and scale factor s for nearly ambient pressure water as a function of Q_{max}. While the overall trends are relatively constant, coupled variations of ρ_0 and s can be seen in the figure. To account for these systematic variations, our reported values of ρ_0 correspond to averages found for Q_{max} ranging from 60 to 95 nm^{-1}. The reported error is the standard deviation.

Figure 4 shows our determination of the density for liquid water at 295 K plotted against the Saul and Wagner [11] equation of state. The open circles represent an empty-

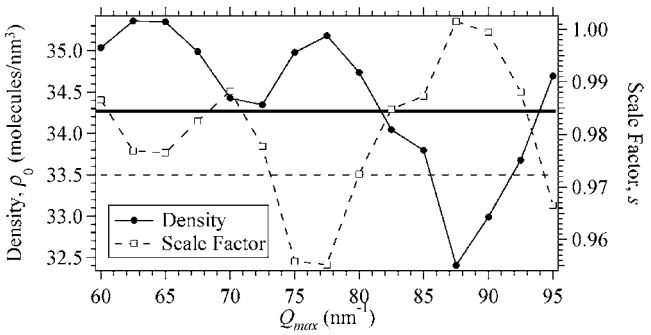

Figure 3. The optimized density and scale factor as a function of the Q cutoff at ambient conditions. The average density is shown by the solid curve, and the density of ambient water by the dashed curve.

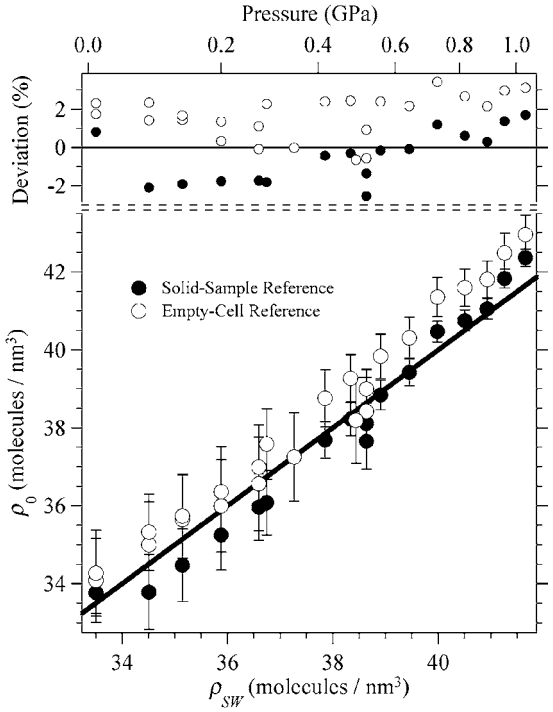

Figure 4. Our experimental determination of the density of liquid water at 295 K plotted against the Saul and Wagner [11] equation-of-state density. The deviation scale shows that our density determination for liquid water has an accuracy of about ±3%.

cell reference, while the solid circles represent a solid-sample reference. The good agreement strongly supports the validity of our solid-sample reference method. The excellent agreement between our measurements and the equation of state suggest that our analysis rests on a sound foundation, and that it is possible to measure the density of low-Z liquids by x-ray diffraction to ∼3% accuracy in DACs. This is the first time that density measurements of liquids have been reported by x-ray diffraction at high pressure, and it opens exciting new possibilities for directly measuring the equation of state of liquids.

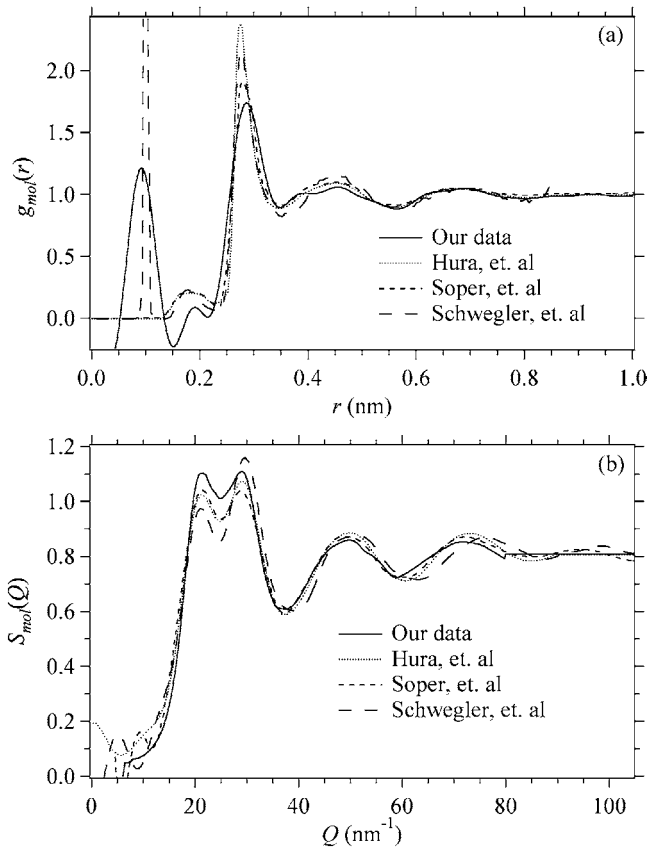

Figure 5. Results of our experiments for ambient pressure (see footnote 3) water and comparison, using (7), to recent experiments by Hura *et al* [12] and Soper *et al* [13] and to first-principles simulations by Schwegler *et al* [14].

Our structure factors $S_{mol}(Q)$ are consistent as a function of Q_{max} while the radial-distribution functions $g_{mol}(r)$ show various amounts of broadening and unphysical oscillations. We believe that our determinations of $S_{mol}(Q)$ are accurate while $g_{mol}(r)$ shows Q_{max} cutoff problems.

To illustrate the accuracy of our method we present a comparison of our results for nearly-ambient-pressure water[3] with recent x-ray [12] and neutron [13] diffraction experiments, as well as a first principles simulation [14] in figure 5. In order to compare our results with previous results, in figure 5(a) we have combined the reported site–site distribution functions according to (7). We used $Q_{max} = 80\,\mathrm{nm}^{-1}$ so that the coefficients are $K_{\mathrm{O}} = 8.96$, $K_{\mathrm{H}} = 0.52$, and $S_{\infty} = 0.808$. The first peak in our $g_{mol}(r)$ at $r = 0.095$ nm is the *intra*molecular-OH peak imposed by our analysis and was not actually measured by us, or in any other diffraction experiment. Since the broadening of this peak in our analysis is entirely due to the Q_{max} cutoff, its width gives a good representation of our experimental resolution. The second peak at $r = 0.18$ nm is the *inter*molecular-OH peak measured in the neutron experiments and the simulations, but not in either x-ray experiment. The dominant peak in our $g_{mol}(r)$ at

[3] The sample was confined in the DAC with no applied force and a measured pressure of 0 ±0.05 GPa. However, it is highly likely that some small pressure remained.

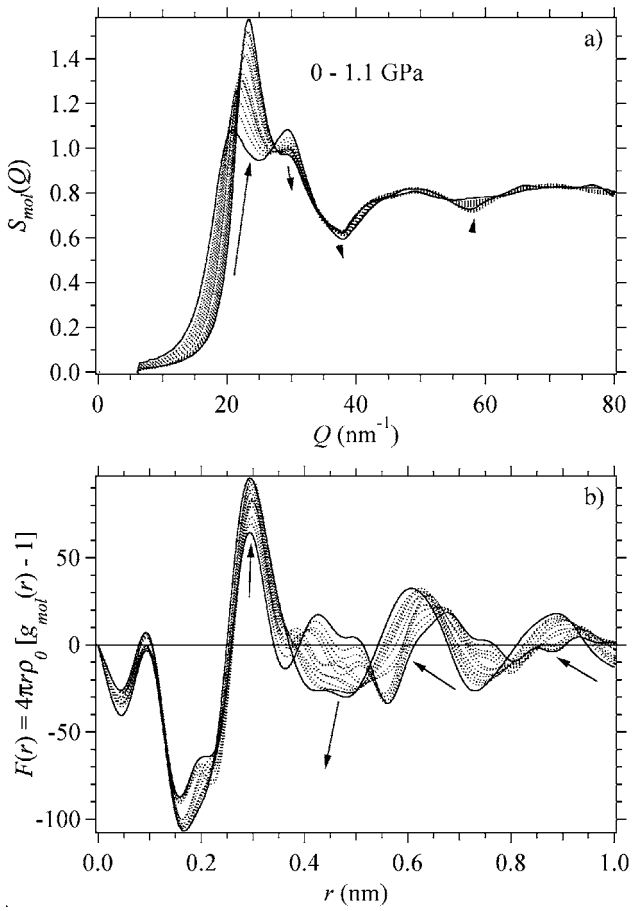

Figure 6. The pressure dependence of our results at room temperature. The arrows denote the changes in the extremae at 0 and 1.1 GPa.

$r = 0.28$ nm is too broad, too weak, and at too high r compared to the other results. However, we believe that these inconsistencies can be explained by our finite Q_{max} since the other experiments were analysed to explicitly eliminate the Q_{max} problem. The similarity in width of our peaks at $r = 0.095$ and 0.28 nm lend support to this view. All the subsequent peaks in $g_{mol}(r)$ are in excellent agreement.

In figure 5(b) we compare our $S_{mol}(Q)$ with those from the same three datasets. To allow a direct comparison, we have performed the inverse Fourier transforms of the $g_{mol}(r)$'s shown in figure 5(a). We find that our determination of $S_{mol}(Q)$ is in excellent agreement with the other experimental structure factors. All of the peak positions are in good agreement and the peak intensities are very nearly so. The small discrepancy in the relative and total intensities of the primary doublet is entirely consistent with a small (<0.05 GPa) applied pressure (see footnote 3).

Figure 6 shows the pressure dependence of $S_{mol}(Q)$ and $F(r)$ for room temperature water from 0 GPa up to the metastable liquid at 1.1 GPa. The arrows show the sense of the changes in the peak positions with increasing pressure. We see a change from a doublet first peak in $S_{mol}(Q)$ to a singlet, and an associated reduction in the peak amplitudes of the subsequent

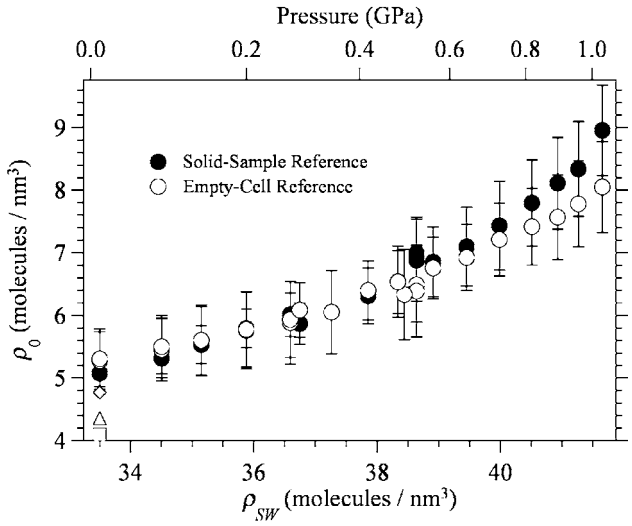

Figure 7. The coordination number as a function of pressure at ambient temperature water. The x-ray [12], neutron [13], and simulation results [14] are shown as the squares, triangles, and diamonds, respectively.

peaks as pressure is increased. As has been observed previously [15], these changes correspond to the collapse of the second-neighbour shell near 0.45 nm nearly into the first shell. We see an associated dramatic downward shift in the peak positions and increase in magnitude of the subsequent peaks in $F(r)$.

Finally, figure 7 shows the coordination number n where

$$n \equiv \rho_0 \int_0^{r_0} g_{mol}(r) 4\pi r^2 \, \mathrm{d}r$$

and r_0 is the position of the first minimum in $4\pi r^2 g_{mol}(r)$. We find a rapid increase with pressure in n from about 5 to about 8 or 9 at freezing. This increase in coordination is due to a combination of two factors, the increase in the amplitude of the first peak and the increase in the position of the first minimum during and after the collapse of the second shell.

7. Conclusion

We have performed the first quantitative measurements of a liquid structure factor in a DAC–water system up to 1.1 GPa. A fortuitous by-product of our analysis is that the bulk density of the liquid can be measured, thereby eliminating a free parameter in all previous high-pressure studies. The density we present is accurate to within about 3% in liquid water. We have performed extensive tests of our analytical method and believe that our structure factors are highly accurate. At this time, we have not developed radial distribution functions with similar levels of accuracy due to the Q_{max} problem, but we are confident that this can be overcome [14].

Acknowledgments

The authors thank M Mezouar, T Le Bihan, and M Hanfland of the ESRF for their valuable assistance in the use of the synchrotron beam lines.

References

[1] Katayama Y, Mizutani T, Utsumi W, Shimomura O, Yamakata M and Funakoshi K 2000 *Nature* **403** 170
[2] Chrichton W A, Mezouar M, Grande T, Stolen S and Grzechnik A 2001 *Nature* **414** 26
[3] Eggert J H, Weck G, Loubeyre P and Mezouar M 2002 *Phys. Rev.* B **65** 174105
[4] LeToullec R, Pinceaux J P and Loubeyre P 1988 *High Pressure Res.* **1** 77
[5] X-ray Research GmbH, www.marresearch.com, Norderstedt Germany
[6] Warren B E 1969 *X-Ray Diffraction* (Reading, MA: Addison-Wesley)
[7] Hajdu F 1972 *Acta Crystallogr.* A **28** 250
[8] Krogh-Moe J 1956 *Acta Crystallogr.* **9** 951
[9] Norman N 1957 *Acta Crystallogr.* **10** 370
[10] Kaplow R, Strong S L and Averbach B L 1965 *Phys. Rev.* **138** A1336
[11] Saul A and Wagner W 1989 *J. Phys. Chem. Ref. Data* **18** 1537
[12] Hura G, Sorenson J M, Glaeser R M and Head-Gordon T 2000 *J. Chem. Phys.* **113** 9140
Sorenson J M, Hura G, Glaeser R M and Head-Gordon T 2000 *J. Chem. Phys.* **113** 9149
[13] Soper A K, Bruni F and Ricci M A 1997 *J. Chem. Phys.* **106** 247
[14] Schwegler E, Galli G and Gygi F 2000 *Phys. Rev. Lett.* **84** 2429
[15] Okhulkov A V, Demianets Y N and Gorbaty Y E 1994 *J. Chem. Phys.* **100** 1578